AFRL-RX-WP-TP-2009-4212

THE MEAN VS LIFE-LIMITING FATIGUE RESPONSE OF A Ni-BASE SUPERALLOY, PART 2: LIFE PREDICTION METHODOLOGY (PREPRINT)

S.K. Jha, M.J. Caton, and J.M. Larsen

Metals Branch
Metals, Ceramics, and NDE Division

SEPTEMBER 2008

AIR FORCE RESEARCH LABORATORY
MATERIALS AND MANUFACTURING DIRECTORATE
WRIGHT-PATTERSON AIR FORCE BASE, OH 45433-7750
AIR FORCE MATERIEL COMMAND
UNITED STATES AIR FORCE

REPORT DOCUMENTATION PAGE

Form Approved
OMB No. 0704-0188

1. REPORT DATE *(DD-MM-YY)*	2. REPORT TYPE	3. DATES COVERED *(From - To)*
September 2008	Journal Article Preprint	

4. TITLE AND SUBTITLE
THE MEAN VS LIFE-LIMITING FATIGUE RESPONSE OF A Ni-BASE SUPERALLOY, PART 2: LIFE PREDICTION METHODOLOGY (PREPRINT)

5a. CONTRACT NUMBER
In-house

5b. GRANT NUMBER

5c. PROGRAM ELEMENT NUMBER
62102F

6. AUTHOR(S)
S.K. Jha (Universal Technology Corporation)
M.J. Caton and J.M. Larsen (AFRL/RXLMN)

5d. PROJECT NUMBER
4347

5e. TASK NUMBER
RG

5f. WORK UNIT NUMBER
M02R3000

7. PERFORMING ORGANIZATION NAME(S) AND ADDRESS(ES)
Universal Technology Corporation
Dayton, OH 45432

Metals Branch (AFRL/RXLMN)
Metals, Ceramics, and NDE Division
Materials and Manufacturing Directorate
Wright-Patterson Air Force Base, OH 45433-7750
Air Force Materiel Command, United States Air Force

8. PERFORMING ORGANIZATION REPORT NUMBER
AFRL-RX-WP-TP-2009-4212

9. SPONSORING/MONITORING AGENCY NAME(S) AND ADDRESS(ES)
Air Force Research Laboratory
Materials and Manufacturing Directorate
Wright-Patterson Air Force Base, OH 45433-7750
Air Force Materiel Command
United States Air Force

10. SPONSORING/MONITORING AGENCY ACRONYM(S)
AFRL/RXLMN

11. SPONSORING/MONITORING AGENCY REPORT NUMBER(S)
AFRL-RX-WP-TP-2009-4212

12. DISTRIBUTION/AVAILABILITY STATEMENT
Approved for public release; distribution unlimited.

13. SUPPLEMENTARY NOTES
Journal article submitted to *Metallurgical and Materials Transactions*. PAO Case Number: 88ABW-2008-0113; Clearance Date: 09 Sep 2008. See also Part 1, technical paper AFRL-RX-WP-TP-2009-4210.

14. ABSTRACT
In Part 1, we showed that the mean fatigue behavior of IN100 separates from the life-limiting response as stress level is decreased. This separation of lifetimes was suggested to be related to the development of heterogeneity levels of local deformation that produce sequential occurrence of "short-lifetime" and the "mean-lifetime" dominating mechanisms. In the current paper, we show that the distribution in the life-limiting mechanism is controlled by small-crack growth from the relevant microstructural scale in the surface region, which explains the significantly less sensitive response of the lower-tail to the stress level, relative to the mean-lifetime behavior. We, therefore, describe the lifetime distribution in terms of superposition of the crack-growth-lifetime probability density and a mean-dominating density. Strategies for obtaining these probability density functions are discussed. A probabilistic life-prediction method is derived from this description and shown to provide significantly better representation of the lower-tail fatigue lifetime behavior, as compared to the traditional approach, and more reliable predictions of the probabilistic lifetime limit as a function of stress level.

15. SUBJECT TERMS
probabilistic fatigue life prediction, small-crack growth, dual response, separation of mechanisms, Ni-base superalloy, IN100

16. SECURITY CLASSIFICATION OF:			17. LIMITATION OF ABSTRACT:	18. NUMBER OF PAGES	19a. NAME OF RESPONSIBLE PERSON (Monitor)
a. REPORT	b. ABSTRACT	c. THIS PAGE			James L. Larsen
Unclassified	Unclassified	Unclassified	SAR	26	19b. TELEPHONE NUMBER *(Include Area Code)* N/A

Standard Form 298 (Rev. 8-98)
Prescribed by ANSI Std. Z39-18

The Mean vs. Life-Limiting Fatigue Response of a Ni-Base Superalloy, Part II: Life-Prediction Methodology

S. K. Jha[1], M. J. Caton, and J. M. Larsen

US Air Force Research Laboratory, Wright-Patterson Air Force Base, OH 45433, USA
[1]Universal Technology Corporation, Dayton, OH 45432, USA

ABSTRACT

In Part I [1], we showed that the mean fatigue behavior of IN100 separates from the life-limiting response as stress level is decreased. This separation of lifetimes was suggested to be related to the development of heterogeneity levels of local deformation that produce sequential occurrence of "short-lifetime" and the "mean-lifetime" dominating mechanisms. In the current paper, we show that the distribution in the life-limiting mechanism is controlled by small-crack growth from the relevant microstructural scale in the surface region, which explains the significantly less sensitive response of the lower-tail to the stress level, relative to the mean-lifetime behavior. We, therefore, describe the lifetime distribution in terms of superposition of the crack-growth-lifetime probability density and a mean-dominating density. Strategies for obtaining these probability density functions are discussed. A probabilistic life-prediction method is derived from this description and shown to provide significantly better representation of the lower-tail fatigue lifetime behavior, as compared to the traditional approach, and more reliable predictions of the probabilistic lifetime limit as a function of stress level.

Keywords: Probabilistic fatigue life prediction, small-crack growth, dual response, separation of mechanisms, Ni-Base superalloy, IN100

1. INTRODUCTION

As discussed in Part I [1], an underlying assumption in the life prediction of fracture critical turbine engine components has been that the lower-tail fatigue behavior is an extrapolation of random deviations from the mean-lifetime [2]. As such, many probabilistic life-prediction modeling approaches tend to be guided by the relationship of the mean-fatigue response to microstructure and loading variables [2-4]. In a recent study [5] we showed that these variables affect the lower-tail (or the life-limiting) behavior and the mean-lifetime to different degrees, producing separation (or convergence) of the two responses. In other materials, we have shown [5] that the life-limiting behavior can be probabilistically described by the crack-growth regime, which explains its much less sensitive response to stress level and other variables. This was suggested [6] to be due to the development of a hierarchy of heterogeneity levels under any given average microstructure and loading condition, which produces a probability of the predominantly crack-growth-controlled mechanism. These heterogeneity levels can be related to the local microstructure. For instance in the $\alpha+\beta$ titanium alloy Ti-6Al-2Sn-4Zr-6Mo (Ti-6-2-4-6), four distinct microstructural configurations were identified, and these were suggested to produce the ranking of heterogeneous deformation scales and sequential operation of the associated failure mechanism [6].

The above description of fatigue variability may represent a new framework in which to assess the role of microstructure and loading variables in the probability of failure. In Ti-6-2-4-6, we have shown that changes in microstructure and test temperature has strong effects on the mean-lifetime but the lower-tail fatigue behavior remains almost unaffected [5], due to its dependence on the crack growth lifetime. The strong role of the crack growth regime in the life-limiting behavior indicates that, for any given microstructure, certain local microstructural

configurations may emerge with some probability, producing a purely crack-growth-controlled mechanism. The probability of such a mechanism will decrease with an increase in the scale of the underlying microstructural configuration and, in many cases, may not be realized in a limited number of experiments. However, a reliable probabilistic life-prediction approach, that is relatively independent of the number of tests, could be based on the crack growth description of the lower-tail behavior [5, 7]. The current paper, therefore, addresses these life-prediction issues with respect to the nickel-based superalloy IN100. We determine the role of crack growth in the separation of the mean-behavior from the life-limiting response and the total lifetime variability. We present a description of fatigue variability in terms of the superposition of the crack growth probability density upon the mean-dominating density. We apply this description in a life-prediction methodology and demonstrate, with examples, the significance of the approach for reliably predicting the probabilistic lifetime limit.

2. ROLE OF SMALL-CRACK GROWTH IN THE LIFE-LIMITING MECHANISM

The details on the material and the experimental procedures have been provided in Part I [1] of the paper. The small and long-crack growth behaviors of IN100 are presented in Fig. 1. The effect of crack initiation from a non-metallic particle (NMP) vs. a pore is illustrated in Fig. 1(a) and the effect of stress level for a given crack initiation mode is shown in Fig. 1(b). The variability in the long-crack growth regime is shown, with the help of a threshold experiment and several constant-K_{max} (where K is the stress intensity factor) type experiments. As shown, the variability in the long-crack growth was not significant, when compared to the total lifetime-variability observed in the stress-lifetime (S-N) space. The small-crack growth rates were obtained from a 3-point sliding polynomial fit to the crack length vs. lifetime data. All small-

crack curves shown in the plots were from naturally-initiated cracks. A small-crack effect [8] is clearly present at this size scale (Fig. 1), such that the cracks grow below the ΔK threshold (ΔK_{th}) for long cracks and also have faster growth rates at the same ΔK level. Secondly, there is a significantly larger degree of variability in the small-crack growth regime when compared to the long-crack regime (Fig. 1).

A comparison of the behaviors of the NMP vs. pore initiated cracks indicates faster growth rates in the former case (Fig. 1(a)). This may be attributable to the tensile residual stress field around a NMP due to the thermal expansion mismatch [9], as well as the elastic incompatibility [10] with the surrounding matrix material. A moderate stress level effect on the small-crack growth rates is also evident from Fig. 1(b). These small-crack growth effects play a very important role in the proposed life prediction modeling and need to be accurately included.

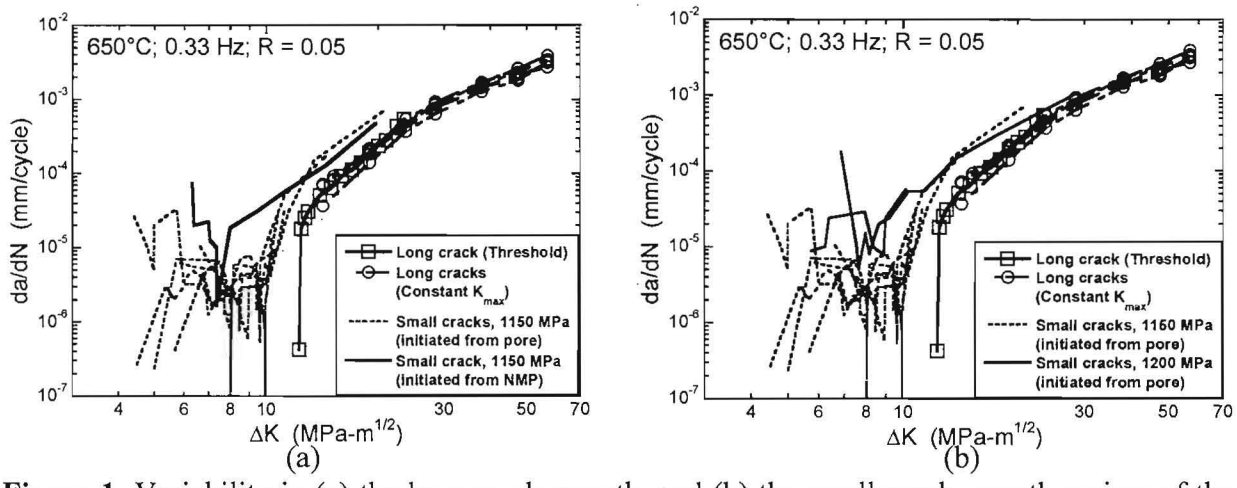

Figure 1: Variability in (a) the long crack growth, and (b) the small crack growth regime of the IN100 material.

The measured crack initiation size distribution [1] and the variability in the small-crack growth regime can be used to evaluate the role of crack growth in the life-limiting mechanism. Towards this end, deterministic calculations were first performed to estimate the upper and lower bounds on crack-growth lifetimes. The bounds corresponded to the slowest and the fastest small-

crack growth rates, in conjunction with the smallest and the largest crack initiation size, respectively. Due to relatively insignificant variability in the long-crack regime, an average long-crack curve was used beyond the ΔK value where the degree of variability in the small-crack behavior was reduced to a level similar as in the long-crack regime.

Forman and Shivakumar [11] proposed a K-solution for the problem of an elliptical surface crack in a solid cylinder, assuming crack extension according to the shape that produced the highest level of K. Accordingly, for tension loading the stress intensity factor, K_I, has the form [11]:

$$K_I = \sigma F(\lambda)\sqrt{\pi a} \tag{1}$$

Where, σ is the applied stress level, a is the maximum crack depth from the surface, and the factor F(λ) is similar to a shape factor and described in [11]. λ is the normalized crack depth a/D, where D is the sample diameter.

The fastest and the slowest small-crack curves were expressed in terms of multiple power-law segments fitted to the respective log(da/dN) vs. log(ΔK) data, as illustrated in Fig. 2. This approach has been adopted in other studies as well [12, 13]. The crack growth lifetime can then be calculated as the total time spent in the small and the long crack regime:

$$N_{FCG} = \int_{a_i}^{a_0} \frac{da}{f(\Delta K)}\bigg|_{small-crack} + \int_{a_0}^{a_f} \frac{da}{f(\Delta K)}\bigg|_{long-crack} \tag{2}$$

where, a_i is related to the crack initiation size measured on the fracture surface, a_0 is the crack depth corresponding to the transition to the long-crack behavior (Fig. 2), and a_f is the final crack depth at the time of fracture. There were cases where the small-crack regime could be best represented by two power-law segments (Fig. 2) and the small crack growth lifetime term in

Eqn. 2 was accordingly composed of two parts. The function $f(\Delta K)$ describes the da/dN - ΔK relationship and is a function of crack depth, a. In the Paris-law [14] form it is expressed as:

$$f(\Delta K) = C\Delta K^m \tag{3}$$

where, C and m are the Paris constants and ΔK is given by Eqn. (1).

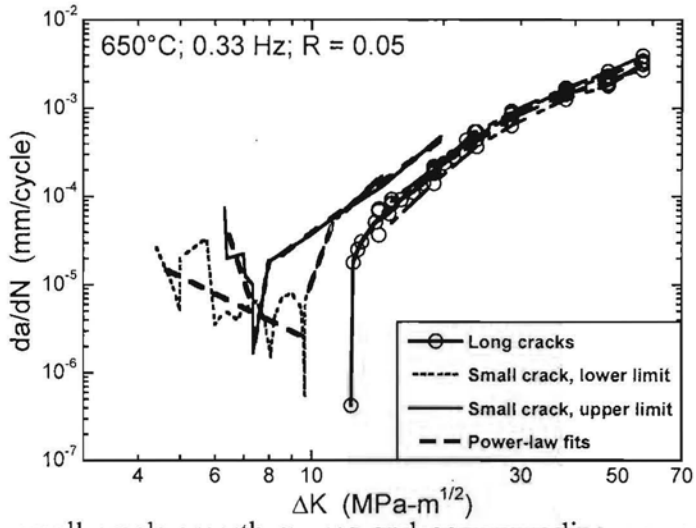

Figure 2: Bounding small-crack growth curves and corresponding power-law fits used in the calculations.

Since the life-limiting behavior corresponded to crack initiation from a NMP, the NMP-initiated small-crack growth behavior should be used in the calculation. However, due to the small frequency of occurrence of this mechanism, only one NMP-initiated small-crack growth curve was available (Fig. 1(a)). As an approximation, the upper and lower bounds on the small crack growth behavior were taken to be the measured NMP-initiated curve and the upper-bound of the pore-initiated small crack growth curves, respectively, as illustrated in Fig. 2. Similarly, due to the limited small-crack growth data at 1200 MPa, the small-crack behavior was assumed to be bounded by the measured upper bound curve at 1200 MPa (Fig. 1(b)) and the upper-limit of the small-crack behavior at 1150 MPa. These approximations were considered reasonable in

representing the shift towards higher growth rates, both under a NMP-related crack initiation and with stress level.

In the calculations, the limits on the initial crack initiation size (a_i) were based on the NMP-related sizes measured in the fractured surfaces. Assuming that the crack attains a near-semi-circular shape within the first few cycles of initiation [15], two different schemes for determining the initial crack size were employed. In these, the a_i was taken as (i) the radius of the semicircle of equivalent area [16], and (ii) the radius of the semicircle circumscribing the crack initiating feature [17].

The results presented in Fig. 3 show the calculated bounds on the crack growth lifetime. The solid lines show the first scheme (radius of equivalent semicircle) and the dotted lines indicate the lifetimes assuming the second scheme (i.e., in terms of the major-axis), considering the surface NMP-initiation at all stress levels. Due to the suggested overlap of the mean and the life-limiting behavior at 1200 MPa [1], the estimated crack growth limits tend to describe the entire range of lifetimes. On the other hand, at the lower stress levels, the predicted bounds on the crack growth lifetimes reasonably describe the life-limiting failure distribution, as well as the minimum lifetime. Although the crack growth bounds contain the life-limiting failures, its range appears wider than seen in experiments. This is attributed to the very limited number of life-limiting observations. The mean lifetime, however, separates from the surface crack-growth-controlled mechanism (Fig. 3) as the stress level is decreased. We see this type of response in other nickel and titanium-based materials [5, 18-20], even in the absence of NMP or pore-related crack initiation, where the life-limiting behavior is controlled by crack growth, producing a separation of the mean-lifetime. These calculations suggest that the variability in the life-limiting mechanism is driven by crack growth from the relevant microstructure scale.

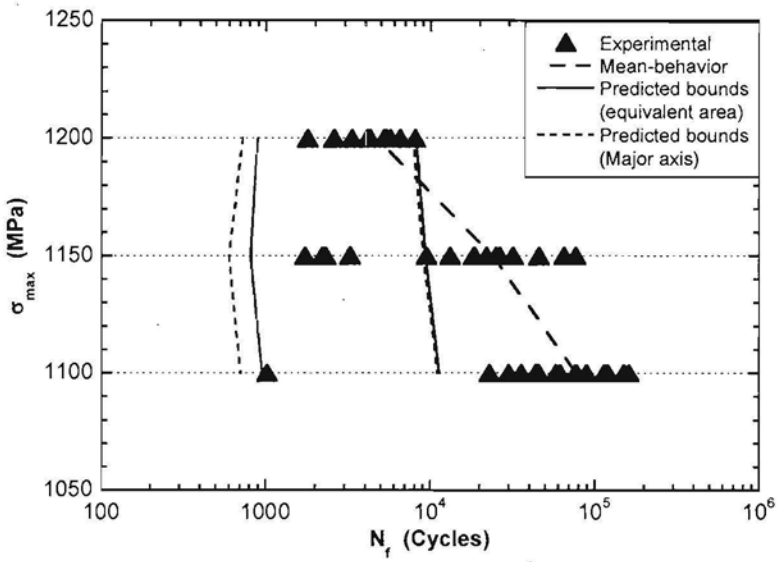

Figure 3: The predicted bounds on the crack growth lifetimes for the surface-NMP-initiated failures.

3. THE LIFE PREDICTION METHODOLOGY

As noted above, the increased lifetime variability with decreasing stress level can be related to the crack-growth control of the life-limiting behavior, resulting in its less sensitive reaction to stress level and the consequent increased separation of the mean-behavior from the crack-growth-controlled response. The separation of the two responses and the dependence of the life-limiting mechanism on crack growth, even in the absence of particle or pore-initiated failures [18, 21, 22], point towards a more fundamental character of fatigue variability behavior. It is hypothesized that under any given microstructure and loading condition, the lower-tail of the fatigue lifetime distribution is controlled by a crack growth dominated mechanism, while the mean-behavior responds at a different (and faster) rate to these variables. Clearly, the number of trials before this dual behavior is revealed will vary in each case, but it is reasonable to suggest that the theoretical possibility of its existence cannot be ignored and needs to be described probabilistically. This is especially relevant from a life-prediction perspective.

3.1 Calculation of the lifetime probability density

The above hypothesis, which is clearly applicable in case of the present IN100 material, allows a breakdown of the total uncertainty in lifetime into the variability in the crack growth lifetime (life-limiting) and the mean-lifetime controlling mechanisms. The total lifetime probability density function (PDF) can, therefore, be described by a superposition of the crack growth density and the mean-dominating density as:

$$f_t(x) = p_l f_l(x) + p_m f_m(x) \tag{4}$$

Where, $f_t(x)$, $f_l(x)$, and $f_m(x)$ are the total PDF, the crack growth PDF (corresponding to the life-limiting mechanism), and the PDF describing the mean-lifetime dominating mechanism, respectively. The individual PDFs, $f_l(x)$ and $f_m(x)$, were taken as the lognormal density. These are weighted by the probability of occurrences, p_l and p_m of the respective responses [19, 23] such that $p_l + p_m = 1$.

3.2 Procedure for calculating $f_l(x)$ and $f_m(x)$

Life-limiting density, $f_l(x)$

In order to derive the total lifetime density, $f_t(x)$, the constituent densities, $f_l(x)$ and $f_m(x)$, were separately calculated and then weighted by suitable probability of occurrences. The crack growth density, $f_l(x)$, can be simulated using the small-crack growth data (Fig. 1(b)) and the distribution in the crack initiation size (measured on the fracture surfaces) reported in Part I [1]. For this purpose, the crack initiation size, shown in Fig. 4(a), was modeled by the lognormal probability density. The small-crack growth rate was correlated to ΔK by power-law segments as illustrated in Fig. 2. This approach averages the fluctuations in growth rate of a given crack but maintains the variation in the rates between different cracks that is attributed to the local microstructural environment. Other approaches that account for the variability in the small crack

growth rates in life prediction have been suggested [24, 25] and can be implemented for the present purpose.

The random variables and their parameters used in the simulation of $f_l(x)$ have been listed in Table I. These were the crack initiation size, a_i and the crack growth variables, C′ and m. The variable C′ is related to the Paris coefficient, C, as $C = e^{C'}$. The maximum likelihood estimate (MLE) was used to obtain the statistical parameters of C′ and m (Table I) from the power-law fits to the experimental small-crack growth curves. For simplicity, in probabilistic calculations, only two segments were used to model the small-crack behavior with a transition crack size between the two segments. This crack depth, a_0, (Table I) was taken to be deterministic and approximately corresponded to the size beyond which all cracks grew at a similar rate. Also, note that ideally a_0 depends on the stress level but due to lack of sufficient data at each stress level it was assumed to be invariant within the range of applied stresses. As given in Table I, a_i was modeled by the lognormal density function, and C′ and m were modeled by the normal density.

The crack growth parameters are strongly correlated as reported in other studies [12, 26]. The correlation coefficient in the present problem was determined to be -0.98. The Monte Carlo simulation therefore, involved sampling from the joint probability density of C′ and m, presented in Fig. 4(b). The crack growth lifetime in each simulation step was calculated according to Eqn. 2. The number of Monte Carlo samples was 10,000, and these were used to construct the crack growth density, $f_l(x)$. Note in Table I that the small-crack growth behavior at 1100 MPa was assumed to be the same as at 1150 MPa. Additional small crack data at these stress levels and under the specific condition of the NMP-initiated cracks would further increase the accuracy of the life-prediction model described here.

Table 1. Variables and parameters used in the simulation of $f_l(x)$

Random Variables (units)	Description	Distribution type	Parameters σ_{max} (MPa) 1100	1150	1200
C1 (m/cycle)	Small crack growth coefficient	Correlated normal*	μ_{C1} = -15.9354 σ_{C1} = 0.7595	-15.9354 0.7595	-8.7921 9.7989
m1	Small crack growth exponent	Correlated normal*	μ_{m1} = -1.2854 σ_{m1} = 0.6522	-1.2854 0.6522	-4.4921 4.7229
C2 (m/cycle)	Small crack growth Coefficient	Correlated normal*	μ_{C2} = -25.9744 σ_{C2} = 0.9707	-25.9744 0.9707	-25.9744 0.9707
m2	Small crack growth coefficient	Correlated normal*	μ_{m2} = 3.8756 σ_{m2} = 0.3475	3.8756 0.3475	3.8756 0.3475
a (μm)	Crack initiation size	Lognormal	μ_a = 3.908 σ_a = 0.286	3.908 0.286	2.977 0.203
Deterministic Variables					
a_0 (μm)	Transition crack depth	Deterministic	50	50	50
a_f (μm)	Crack depth at fracture	Deterministic	1228	1178	1132

*Correlation coefficient, ρ = -0.98

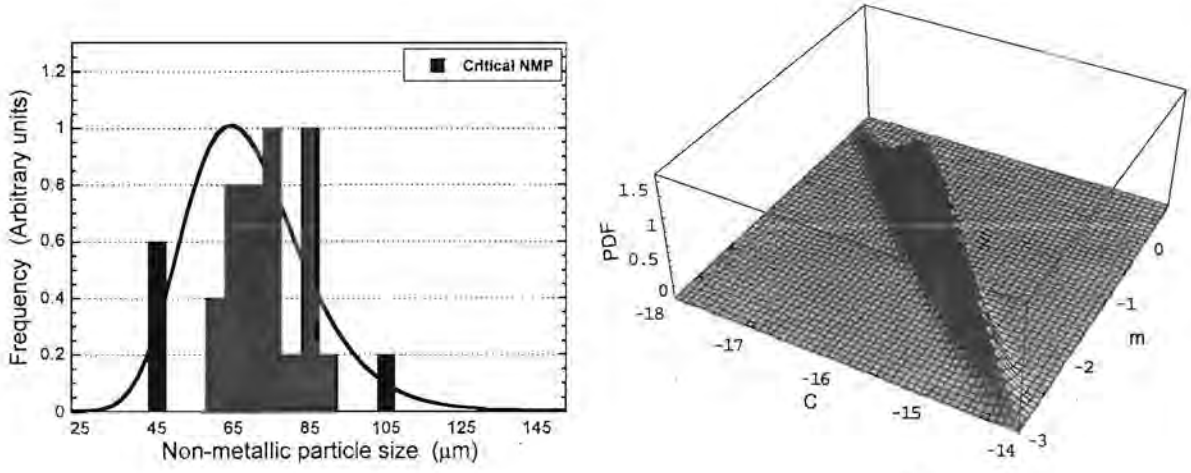

(a) (b)

Fig. 4: Example of inputs to the simulation of the crack growth density, $f_l(x)$; (a) Crack initiation size distribution and (b) joint probability density of C and m. -

The CDFs corresponding to the simulated crack growth densities ($f_l(x)$) are compared to experiment in Fig. 5. At 1200 MPa (Fig. 5(a)), the calculated CDF agreed well with the experiments. The disagreement between the slopes of simulated and experimental CDF could be due the limited small-crack data used as input. At 1150 and 1100 MPa, the crack growth density reasonably described the life-limiting response. At 1150 MPa (Fig. 5(b)), this is illustrated by plotting the experimental life-limiting points as a separate distribution. Notably, the solitary life-limiting point at 1100 MPa (Fig. 5(c)) is accounted for by this approach. This may otherwise necessitate a large number of S-N fatigue experiments to reveal, depending on the probability of occurrence.

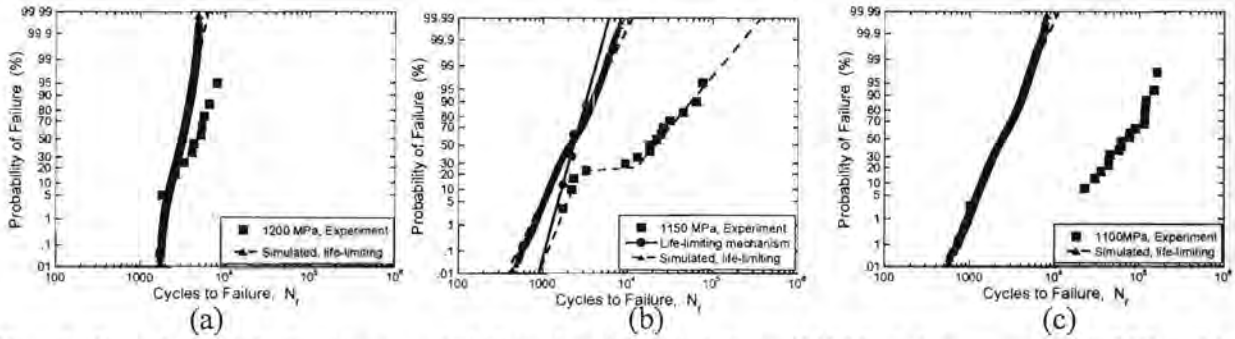

Fig. 5: Simulated life-limiting probability densities ($f_l(x)$) in IN100; (a) σ_{max} = 1200 MPa, (b) σ_{max} = 1150 MPa, and (c) σ_{max} = 1100 MPa.

Mean-dominating density, $f_m(x)$

The mean-dominating density, $f_m(x)$, was calculated from 4 randomly selected total lifetime experiments at each stress level. This is illustrated in Fig. 6. The MLE was then used to determine the parameters of $f_m(x)$, given in Table I. It is to be noted that the mean fatigue response is the conventionally characterized behavior and used for the purpose of material design, as well as for life prediction. Such data, if available, can also be used with suitable statistical analysis to derive $f_m(x)$.

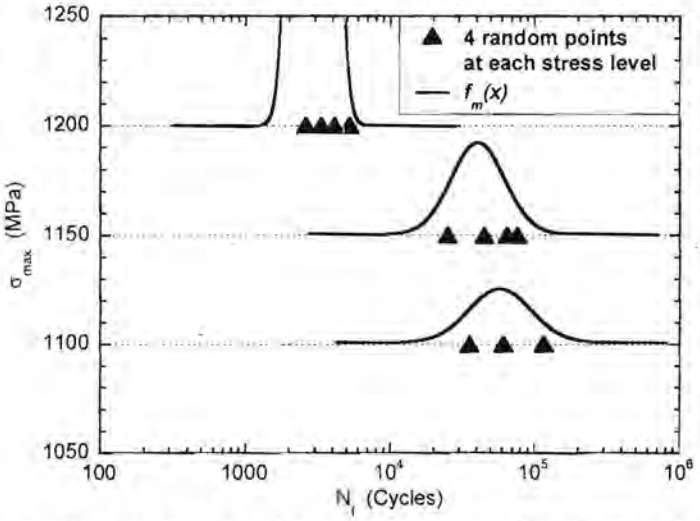

Fig. 6: Illustration of the calculation of the mean-dominating density, $f_m(x)$

3.3 Predicted lifetime densities and probabilistic limits

The calculated lifetime probability densities are shown in Fig. 7, and the corresponding CDFs are presented in Fig. 8. Here, the weighting factors, p_l and p_m, were obtained from the S-N experiments and are listed in Table I. However, it can be shown that the lower tail of the lifetime density and the probabilistic limit (for e.g., the B0.1 lifetime or a 1 in 1000 probability of failure) is very weakly affected by p_l or p_m within a reasonable range of values [7]. Furthermore, in the limiting case (i.e., when $p_l \rightarrow 1$), the B0.1 lifetime obtained from the crack growth density, $f_l(x)$, forms the lower-bound of the B0.1 lifetime predicted by the bimodal density [7]. Therefore, although the factors, p_l and p_m, are important in accurately describing the total lifetime density and the effect of material and extrinsic variables on the lifetime variability, these do not significantly affect the calculation of the probabilistic lifetime limit.

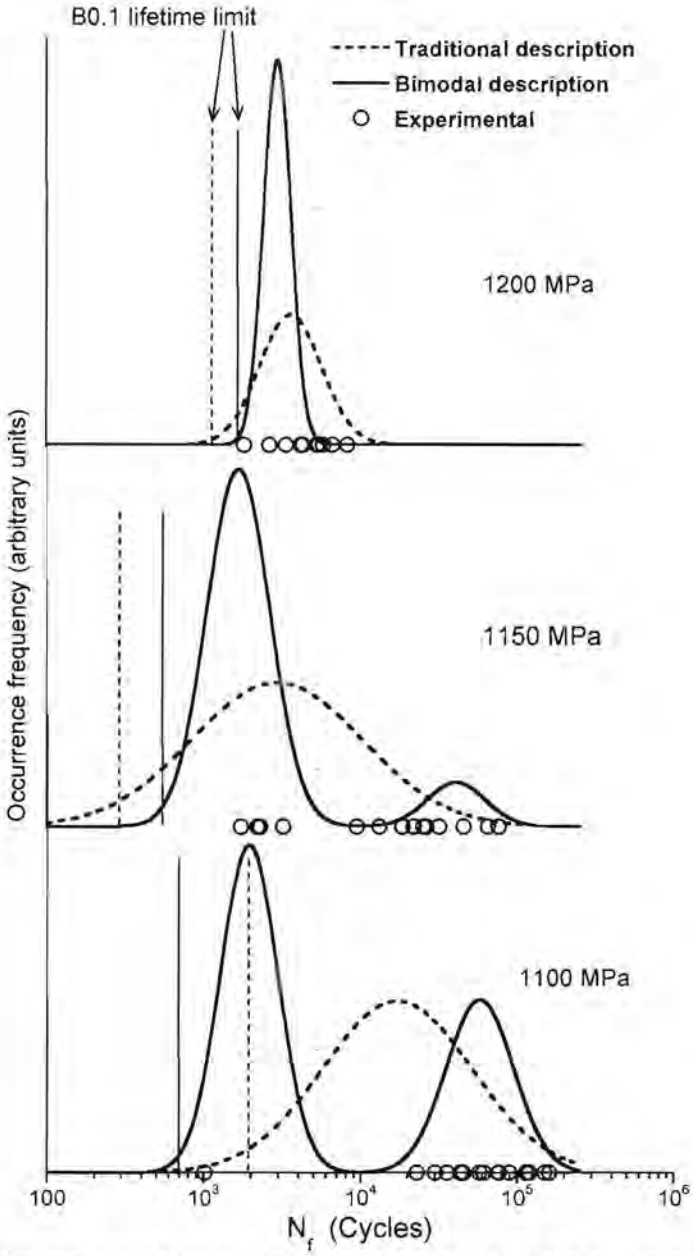

Fig. 7: The calculated lifetime densities and the B0.1 lifetimes with respect to stress level in IN100.

In Fig. 7, the traditional description of fatigue variability, where the lower tail of the distribution is assumed to result from random deviations from the mean behavior, has also been plotted for comparison. The B0.1 lifetimes have been indicated by vertical lines and the

experimental points are represented by open symbols. Figures 7 and 8 clearly indicate that the suggested lifing model provides a significantly better representation of the fatigue variability behavior. This is particularly evident from Fig. 8, where the experimental points show reasonable agreement with the calculated CDFs for the p_l values listed in Table I. The calculated lifetime densities appear to effectively capture the effect of stress level on the lifetime variability, indicated by both Figs. 7 and 8. At 1200 MPa, the densities, $f_l(x)$ and $f_m(x)$ overlap and can be considered to be indistinguishable from one another. With decreasing stress level, the separation between the two PDFs increases (Fig. 7), promoting the increased lifetime variability.

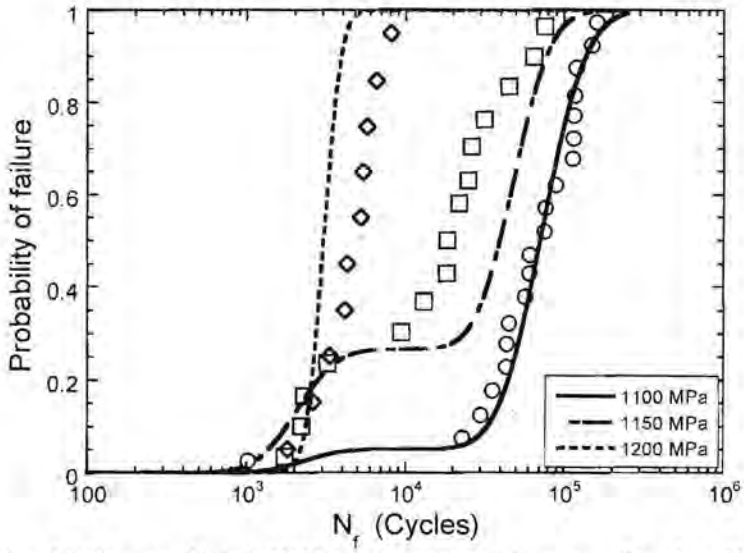

Fig. 8: The predicted CDFs with respect to stress level in IN100.

An even more relevant outcome of this approach can be the consistency in prediction of the probabilistic lifetime limit or the B0.1 lifetime. In the conventional description (Fig. 7), the B0.1 lifetimes show a physically counterintuitive trend with respect to stress level [1], besides being heavily dependent on the number of experiments. For example, in the traditional approach, the B0.1 lifetime appears to vary from an overly-conservative value at 1150 MPa to a non-conservative value at 1100 MPa. On the other hand, Fig. 7 illustrates that the proposed model

produces, perhaps, a physically consistent trend in the B0.1 lifetime as a function of the stress level, and its prediction is almost independent of the total number of fatigue experiments, thereby significantly decreasing the uncertainty in the probabilistic limit. To be noted that the calculated life-limiting density, $f_l(x)$, at 1200 MPa corresponds to crack initiation from pores. On the other hand, simulation of $f_l(x)$ at 1150 and 1100 MPa is based on crack initiation from NMP. Since the crack-initiating NMP sizes are larger than the pore sizes, the B0.1 lifetime at 1150 MPa is predicted to be lower than at 1200 MPa. This is consistent with the deterministic calculations of lower bounds at these stress levels presented previously. As stated earlier, Fig. 7 also shows that the bimodal lifetime density accounts for the single life-limiting failure at 1100 MPa, detection of which may require a large number of experiments due to its low frequency of occurrence. Note, however, that the experiments alone are not sufficient in accurately predicting the B0.1 lifetime without the key understanding of the role of the separation of the mean behavior from the crack-growth-controlled response in the lifetime variability.

The above method also suggests that, from the perspective of predicting the probabilistic lifetime limit, the crack growth density, $f_l(x)$ is sufficient. This is because, the B0.1 lifetime from the proposed lifetime density is lower-bounded by the probabilistic limit derived from $f_l(x)$. This is illustrated in Fig. 9 with the help of the data at 1150 MPa. The crack growth density is compared to the calculated total lifetime density, $f_l(x)$, and also to the traditional description. The PDFs and the corresponding CDFs are shown in the bottom and the top plot, respectively. The B0.1 lifetimes have been indicated. Expectedly, the B0.1 lifetimes predicted by the crack growth density and the bimodal lifetime density are similar. With respect to the traditional description of fatigue variability, the crack growth density produces a more accurate, but also a more reliable B0.1 lifetime, irrespective of the number of total-lifetime experiments. This creates the potential

for a significant reduction in uncertainty in probabilistic lifetime-limit prediction, as indicated in Fig. 9.

This paper is concerned with demonstrating the concept of separation of the mean vs. the crack-growth-controlled life-limiting behavior, in describing the effect of stress level on the lifetime distribution and the probabilistic lifetime limit in IN100. The same framework can be applied to predict the effect of a host of other variables, such as the microstructure and the dwell time, on the probabilistic limit. This, coupled with the ability to obtain multiple small-crack growth curves from a single experiment by artificial crack initiation from Focussed Ion Beam (FIB) machined notches [27] may further enable a very efficient and reliable prediction of the effect of both the intrinsic and the extrinsic variables on the probabilistic lifetime-limit.

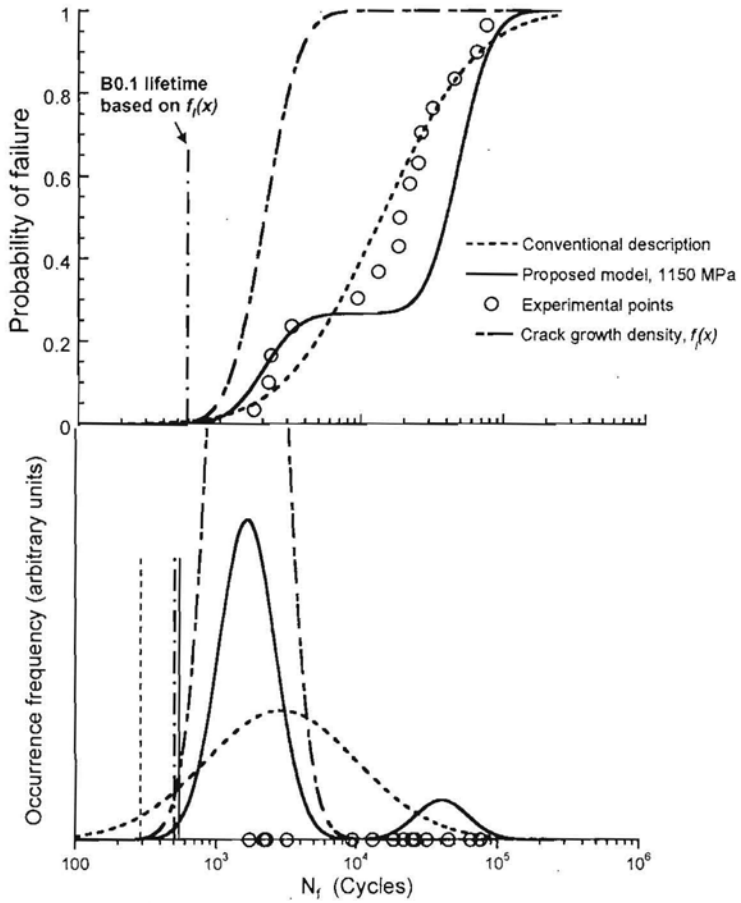

Fig. 9: Illustration of the proposed life prediction approach based on the crack growth density compared to the total lifetime density (σ_{max} = 1150 MPa).

4. CONCLUSIONS

The following main conclusions can be drawn from this study:

(i) It may not be accurate to deduce the lower-tail of the fatigue lifetime variability from an extrapolation of the deviations about the mean behavior.

(ii) The lower-tail of the lifetime distribution of the IN100 material can be described by a crack growth probability density that is superimposed upon the mean-lifetime dominating density to produce the total fatigue variability description.

(iii) The increase in lifetime variability with decreasing stress level is suggested to be due to the weak response of the crack-growth controlled density to stress level coupled with a stronger response of the mean-dominating density to stress level, producing increased separation between the two.

(iv) The crack growth PDF is simulated using the small-crack growth data and the distribution in the crack initiation size and applied in a life-prediction method. This produces a more reliable probabilistic lifetime limit almost independent of the number of total-lifetime experiments, and which resolves the physically anomalous trends in the lifetime-limit with respect to stress level.

ACKNOWLEDGEMENTS

This work was performed at the Air Force Research Laboratory, Materials and Manufacturing Directorate, Wright-Patterson Air Force Base, OH. The partial financial support of the Defense Advanced Research Project Agency (DARPA) under DARPA orders M978, Q588, P699, and S271 with Dr. Leo Christodoulou as the program manager is gratefully acknowledged. Essential

support was also provided by the Air Force Office of Scientific Research (AFOSR) with Dr. Victor Giurgiutiu as the program manager. We acknowledge Mr. Phil Buskohl and Ms. Lindsey Selegue for their assistance with the replication-based small-crack growth experiments.

REFERENCES

[1] S. K. Jha, M. J. Caton, and J. M. Larsen, Part I of this paper.

[2] J. N. Yang and W. J. Trapp, *AIAA Journal*, Vol. 12, pp. 1623-1630, 1974.

[3] R. Tryon and A. Dey, *J. Aerospace Engng.*, p.120, 2001.

[4] K. S. Chan and M. P. Enright, *Journal of Engineering for Gas Turbines and Power*, Vol. 124, pp. 889-885, 2006.

[5] S. K. Jha, M. J. Caton, and J. M. Larsen, *Materials Science and Engineering A*, Vol. A468-470, pp. 23-32, 2007.

[6] S. K. Jha and J. M. Larsen, in *Very High Cycle Fatigue, VHCF-4*, 2007.

[7] S. K. Jha, J. M. Larsen, and A. H. Rosenberger, in review, *Engineering Fracture Mechanics.*

[8] J. Lankford, T. S. Cook, and G. P. Sheldon, *Int. J. Fracture*, Vol. 17, pp. 143-155, 1981.M.

[9] M. Shenoy, R. S. Kumar, and D. L. McDowell, *Int. J. Fatigue*, Vol. 27, p. 113, 2005.

[10] R. Bullough and L. C. Davis, *Acta Materialia*, Vol. 43, p. 2737, 1995.

[11] R. G. Forman, and V. Shivakumar, in *Fracture Mechanics: 17th Volume*, ASTM STP 905, J. H. Underwood, R. Chait, C. W. Smith, D. P. Wilhem, W. A. Andrews, and J. C. Newman, Eds., ASTM, Philadelphia, pp. 59-74, 1986.

[12] J. Luo, and P. Bowen, *Acta Materialia*, Vol. 51, p. 3521, 2003.

[13] J. Luo, and P. Bowen, *Acta Materialia*, Vol. 51, p. 3537, 2003.

[14] P. C. Paris and F. Erdogan, *J. Basic Engineering, Trans. ASME*, Series D, Vol. 85, pp. 528-534, 1963.

[15] K. Gall, M. F. Horstemeyer, B. W. Denger, D. L. McDowell, and J. Fan, *Int. J. Fracture*, Vol. 108, pp. 207-233, 2001.

[16] J. C. Newman, Jr., E. P. Phillips, and H. M. Swain, *Int. J. Fatigue*, Vol. 21, pp. 109-119, 1999.

[17] E. A. DeBartolo and B. M. Hillberry, *Int. J. Fatigue*, Vol. 23, p. S79, 2001.

[18] S. K. Jha, J. M. Larsen, and A. H. Rosenberger, *Acta Materialia*, Vol. 53, p. 1293, 2005.

[19] S. K. Jha, J. M. Larsen, A. H. Rosenberger, and G. A. Hartman, *Scripta Materialia*, Vol. 48, pp. 1637-1642, 2003.

[20] S. K. Jha, J. M. Larsen, and A. H. Rosenberger In: *Fatigue 2006*, International Fatigue Congress, Atlanta, GA, 2006.

[21] S. K. Jha, J. M. Larsen, and A. H. Rosenberger, *JOM*, p. 50, Sep 2005.

[22] M. J. Caton, S. K. Jha, J. M. Larsen, and A. H. Rosenberger, In: *Superalloys 2004.*

[23] A. H. Fischer, A. Abel, M. Lepper, A. E. Zitzelsberger, and A. von Glasgow, *Microelectronics Reliability*, Vol. 47, pp. 445, 2001.

[24] M. D. Halliday, C. Cooper, P. Poole, and P. Bowen, *Int. J. Fatigue*, Vol. 25, pp. 709-718, 2003.

[25] M. E. Robinson and M. J. Crowder, *IEEE Transactions on Reliability*, Vol. 51, pp. 216 – 222, 2002.

[26] C. G. Annis, Jr., in *Probabilistic Aspects of Life Prediction*, ASTM-STP 1450, W. J. Johnson and B. M. Hillberry, Eds., ASTM International, West Conshohocken, PA, 2003.

[27] S. K. Jha, M. J. Caton, J. M. Larsen, and A. H. Rosenberger, in *Materials Damage Prognosis*, TMS Publications, 2005.